FULL PAPER

CrossMark

Source characteristics of moderate-to-strong earthquakes in the Nantou area, Taiwan: insight from strong ground motion simulations

Yi-Ying Wen[1]*, Shen-Yu Chao[1], Yin-Tung Yen[2] and Strong Wen[1]

Abstract

In Taiwan, the Nantou area is a seismically active region where several moderate events have occurred, causing some disasters during the past century. Here, we applied the strong ground motion simulation with the empirical Green's function method to investigate the source characteristics for the eight moderate blind-fault events that struck the Nantou area in 1999 and 2013. The results show that for these Nantou events, a high stress drop and focal depth dependence were noted, which might be related to the immature buried fault in this area. From the viewpoint of seismic hazard prevention and preparation, future earthquake scenarios that include high stress drop should be applied to more analyses, especially the moderate-to-large events originating from the immature blind faulting.

Keywords: Stress drop, Strong motion generation area, Buried fault

Background

The four moderate-sized earthquakes that occurred in 1916 ($5.5 \leq M_L \leq 6.8$, Fig. 1; Cheng et al. 1999) caused some damage and casualties in the Nantou area in the central part of Taiwan. Following the 1999 M_w 7.6 Chi-Chi earthquake, several events with $M_w \geq 6.0$ occurred around this region. Then, two moderate-sized events struck the Nantou area again on 27 March 2013 (M_L 6.2) and 02 June 2013 (M_L 6.5). Although there are some active faults surrounding the Nantou area, these eight moderate-sized events that occurred in 1999 and 2013 (Fig. 1, Table 1) were mostly motivated by the thrust movement of the blind faults and resulted in strong ground shaking in the central and southern regions of Taiwan. No surface rupture induced directly by source rupture can be found in the area, especially around the epicenter location. These eight events provide a good opportunity to investigate strong ground motion

characteristics for similar-sized blind-fault earthquakes in a specific tectonic setting.

Over the past several decades, source modeling with the empirical Green's function method (EGFM) (e.g., Irikura 1986; Miyake et al. 2003; Kurahashi and Irikura 2010; Wen et al. 2014; Yen et al. 2014) has been applied frequently to explore the near-source characters and to simulate the broadband strong ground motions with a frequency range up to approximately 10 Hz. In this study, using the EGFM, we estimate the strong motion generation area (SMGA) and the stress drop by sequence. The results indicate that these eight events seem to follow a certain self-similar scaling relationship with smaller SMGAs and higher stress drop, which could be related to the immature buried fault, indicating that we should give greater consideration to this seismically active region for the mitigation of any future seismic hazards.

Data and methodology

Wen et al. (2014) analyzed the source properties of the 2013 Nantou blind-thrust earthquakes (E7 and E8 events in this study) by broadband ground motion simulation, and the results showed that these two nearby events, with

*Correspondence: yiyingwen@gmail.com
[1] Department of Earth and Environmental Sciences, National Chung-Cheng University, Chia-Yi County 62102, Taiwan
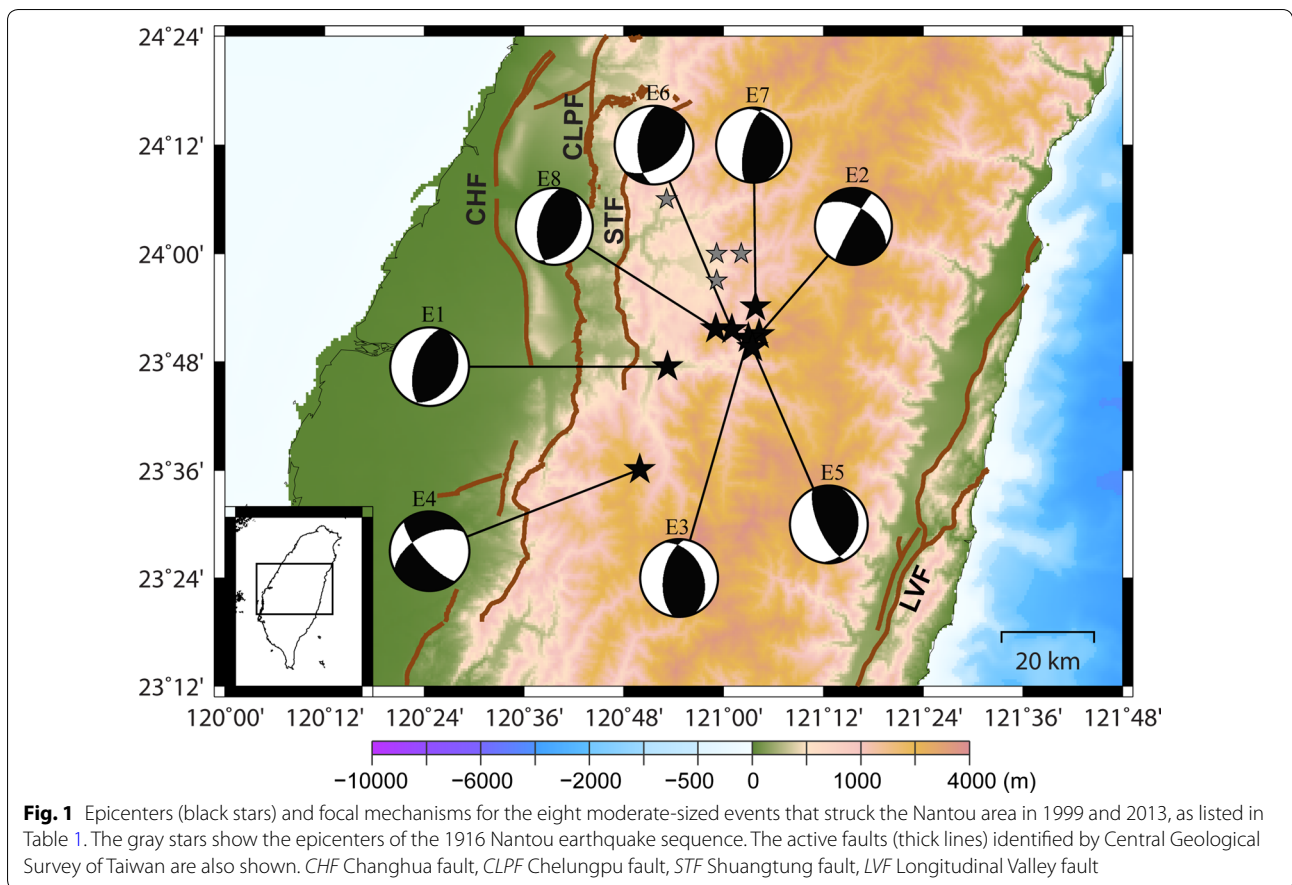Full list of author information is available at the end of the article

Wen *et al. Earth, Planets and Space* (2017) 69:132

Page 2 of 9

Fig. 1 Epicenters (black stars) and focal mechanisms for the eight moderate-sized events that struck the Nantou area in 1999 and 2013, as listed in Table 1. The gray stars show the epicenters of the 1916 Nantou earthquake sequence. The active faults (thick lines) identified by Central Geological Survey of Taiwan are also shown. *CHF* Changhua fault, *CLPF* Chelungpu fault, *STF* Shuangtung fault, *LVF* Longitudinal Valley fault

Table 1 Earthquake parameters for the target events and EGF events determined by CWB

No.	Date (UT)	Long. (°)	Lat. (°)	Depth (km)	M_L
E1	1999/09/20 18:03	120.86	23.80	9.75	6.6
a1	1999/10/04 12:26	120.93	23.79	8.31	5.1
E2	1999/09/20 18:11	121.07	23.86	12.50	6.7
a2	2004/02/15 13:32	121.05	23.93	25.22	3.9
E3	1999/09/20 18:16	121.04	23.86	12.53	6.7
a3	2000/08/02 08:34	121.02	23.85	10.75	5.0
E4	1999/09/20 21:46	120.86	23.58	8.57	6.6
a4	2001/02/14 22:25	120.72	23.58	18.25	4.5
E5	1999/09/22 00:14	121.05	23.83	15.59	6.8
a5	1999/10/24 02:39	121.14	23.89	24.85	4.6
E6	1999/09/25 23:52	121.01	23.85	12.06	6.8
a6	1999/10/04 12:26	120.93	23.79	8.31	5.1
E7	2013/03/27 02:03	121.05	23.90	19.43	6.2
a7	2011/06/26 13:19	121.00	23.85	14.78	5.0
E8	2013/06/02 05:43	120.97	23.86	14.54	6.5
a8	2011/06/26 13:19	121.00	23.85	14.78	5.0

similar focal mechanisms, displayed significant variation in rupture behavior and stress drop. To investigate the detailed source characteristics of events in the Nantou area, we further included six large aftershocks ($M_L \geq 6.0$) of the 1999 Chi-Chi earthquake in our analyzed samples with the broadband ground motion simulation. We used free-field strong motion data maintained by the Central Weather Bureau (CWB). For each investigated event (target event), a small event that had a similar focal mechanism and hypocenter location to the respective target event was chosen as the empirical Green's function (EGF event), and 8–10 stations were selected based on the azimuth coverage and the quality of seismograms for both the target and the EGF events.

The empirical Green's function method is a well-known and conventional technique for studying the source properties of earthquakes by canceling out the effects of site amplification and propagation path (e.g., Velasco et al. 1994; Irikura and Kamae 1994; Lay and Wallace 1995; Ammon et al. 2005). Here, we applied EGFM to determine SMGA, which can be considered the characteristic

Wen *et al. Earth, Planets and Space* (2017) 69:132

Page 3 of 9

area with a uniform, high slip velocity within the total rupture plane (Miyake et al. 2003). The optimal parameters related to the SMGA were validated by a grid search analysis to minimize the residuals between the observed and synthetics for the displacements and the envelopes of the acceleration (Miyake et al. 1999), including the initiation position (rupture starting point), the size of the SMGA, the rupture velocity (V_r) and the rise time (τ).

The procedure of EGFM mainly follows the study of Miyake et al. (2003). The numerical equation to sum records of small events is:

$$U(t) = C \sum_{i=1}^{N} \sum_{j=1}^{N} \frac{r}{r_{ij}} F(t - t_{ij}) * u(t). \tag{1}$$

In Eq. 1, $U(t)$ and $u(t)$ mean the synthetic waveform for the target event and the observed waveform for the small event. N and C indicate the ratios of the fault dimensions and stress drops, respectively, between the target and the small events. The asterisk ($*$) represents convolution. The correction function, $F(t)$, adjusts the difference in the slip velocity time functions between the target and EGF events.

Miyake et al. (1999) proposed the source spectral ratio fitting method to approximate the observed source spectral ratio between the target and small events using a theoretical source spectral ratio function, which obeys the omega-squared source model of Brune (1970, 1971):

$$\text{SSRF}(f) = \frac{M_0}{m_0} \cdot \frac{1 + (f/f_{ca})^2}{1 + (f/f_{cm})^2}. \tag{2}$$

M_0/m_0 represents the seismic moment ratio between the target and small events at the lowest frequency. f_{cm} and f_{ca} indicate the corner frequencies of the target and small events, respectively. Following the formulas from Irikura (1986) and Miyake et al. (2003)

$$U_0/u_0 = M_0/m_0 = CN^3, \quad N = f_{ca}/f_{cm}, \tag{3}$$

the constant flat levels of the acceleration spectra and displacement spectra of the target and small events can be derived. Then, we can calculate the two scaling parameters: N and C. Here, U_0/u_0 is the ratio between the target and small earthquakes for the constant flat levels of the displacement spectra. Using the weighted least-squares approach (Miyake et al. 1999, 2003), we can calculate those parameters in (3). Considering the possible rupture directivity effect (Miyake et al. 2001), using event E1 as an example to show a procedure for broadband ground motion simulation, we selected four stations in different azimuths to obtain the observed source spectral ratios (solid triangles in Fig. 2a). The entire *S*-wave was used to calculate the vector summation of the three-component

amplitude spectra. Then, the mean observed source spectral ratio was used in the source spectral ratio fitting analysis (as shown in Fig. 2 for E1–E6 events and referring to Wen et al. 2014 for E7–E8 events) to obtain the parameters N and C, as listed in Table 2.

The static stress drop can be calculated using the relationship among the seismic moment, the equivalent radius of the rupture area and the stress drop. We then estimated the static stress drop of these eight Nantou earthquakes from the SMGA and the seismic moment (Madariaga 1979; Boatwright 1988; Miyake et al. 2003; Table 1):

$$\Delta\sigma_{\text{SMGA}} = \frac{7}{16} \cdot \frac{M_0}{Rr^2}, \tag{4}$$

where r represents the equivalent radius for the SMGA (SMGA $= \pi r^2$) and R indicates the equivalent radius of the total rupture area, S ($S = \pi R^2$). We estimated S of these eight events from the inversion models of previous studies (Yen 2002; Chi and Dreger 2004; Lee et al. 2015) according to the trimming criteria of Somerville et al. (1999).

Results

SMGA can be divided into $N \times N$ equivalent-sized subfaults with the same rupture area of the EGF event. The optimal parameters of SMGA, as listed in Table 2, were validated by the comparison between the reproduced broadband synthetic near-source strong ground motions and the observations in a frequency range of 0.25–10 Hz. Using event E1 as an example, Fig. 3a shows the comparison of the observed and synthetic waveforms at four stations using source spectral ratio fitting (solid triangles in Fig. 2a). We also applied the forward modeling (with the same set of parameters in source modeling) to the other stations (open triangles in Fig. 2a) to validate the applicability of the SMGA model. Comparison of the observed and synthetic waveforms is shown in Fig. 3b. In addition, Fig. 4 shows the comparison of the observed and synthetic waveforms at stations used for the forward simulations of E2–E6 events. The inaccuracy of both the focal mechanism and attenuation effect might introduce errors into the amplitudes of synthetic waveforms. The soil nonlinear response during strong shaking is also an important factor. Nevertheless, the main characteristics of the observed waveforms could be well reproduced in the broadband range. Considering the multiple phases probably generated by two or more asperities, the analysis with multiple SMGAs could be considered for more comprehensive investigations in the future.

Figure 5a shows the source scaling relationship between the seismic moment to the SMGA, as listed in Table 2. The solid line in Fig. 5a represents the empirical
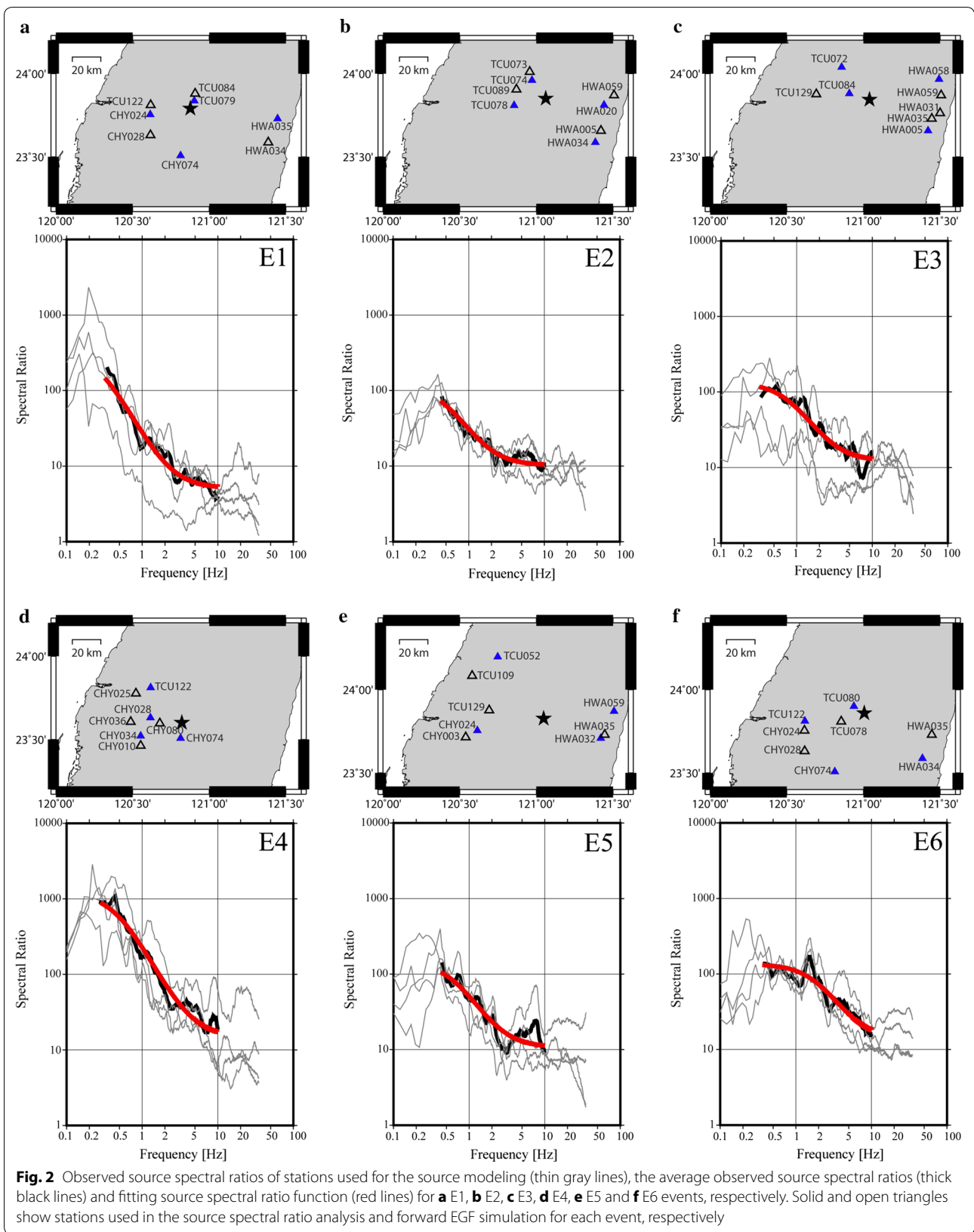
Wen *et al. Earth, Planets and Space* (2017) 69:132

Page 4 of 9

Fig. 2 Observed source spectral ratios of stations used for the source modeling (thin gray lines), the average observed source spectral ratios (thick black lines) and fitting source spectral ratio function (red lines) for **a** E1, **b** E2, **c** E3, **d** E4, **e** E5 and **f** E6 events, respectively. Solid and open triangles show stations used in the source spectral ratio analysis and forward EGF simulation for each event, respectively

Wen *et al. Earth, Planets and Space* (2017) 69:132

Page 5 of 9

Table 2 Source parameters determined by source spectral ratio fitting analysis and strong ground motion simulation in this study

No.	M_0 (10^{18} Nm)	N	C	Rupture starting point[a]	L^b (km)	W^c (km)	V_r (km/s)	τ^d (s)	S^e (km^2)	SMGA (km^2)	$\Delta\sigma_{SMGA}^f$ (MPa)
E1	2.53[g]	8	0.65	(7, 7)	7.2	4.0	3.1	0.96	121[g]	28.80	19.5
E2	5.76[h]	4	2.90	(3, 4)	6.8	4.4	2.6	0.40	728[h]	29.92	17.4
E3	5.45[h]	4	3.72	(1, 4)	3.6	6.8	3.1	0.40	336[h]	24.48	29.6
E4	2.20[g]	9	1.67	(4, 8)	6.3	2.7	2.8	0.81	308[g]	17.01	18.0
E5	2.50[g]	4	3.89	(3, 2)	2.0	5.2	2.7	0.16	567[g]	10.40	24.6
E6	3.70[g]	4	2.96	(4, 3)	2.8	9.2	2.7	0.28	340[g]	25.76	19.0
E7	1.69[i]	3	2.22	(1, 3)	3.9	2.7	3.2	0.27	288[i]	10.53	23.0
E8	2.93[i]	4	2.55	(4, 4)	5.2	3.6	2.9	0.36	378[i]	18.72	19.6

[a] Rupture starting point defined as initiation number of *N* along the strike and dip, respectively

[b] Length of the SMGA

[c] Width of the SMGA

[d] Rise time for the mainshock

[e] Total rupture area estimated from different studies according to Somerville et al. (1999)

[f] Stress drop of the SMGA

The seismic moment was estimated by [g] Chi and Dreger (2004), [h] Yen (2002), [i] Lee et al. (2015)

relationship between the seismic moment and the combined area of characterized asperities for the inland crustal earthquakes proposed by Somerville et al. (1999). The SMGAs of these eight Nantou events seem to be smaller and follow certain self-similar scaling relationships with a higher stress drop. The estimated stress drops on SMGA ($\Delta\sigma_{SMGA}$) mostly range between 18 and 30 MPa, as listed in Table 2.

Discussion and Conclusion

SMGA is considered to spatially coincide with almost the same area as the characterized asperity, which has slip of 1.5 times (or more) larger than the average slip over the fault plane of the waveform inversion model by Miyake et al. (2003) (circles in Fig. 5a). However, our result shows that the SMGAs of these eight Nantou events are much smaller than the predicted dimension (S_a) from the empirical relationship by Somerville et al. (1999). Here, our results are compared with previous studies for the inland crustal earthquakes and shallow intraslab earthquakes in Japan, marked as circles and triangles in Fig. 5, respectively (Asano et al. 2003; Miyake et al. 2003). It seems that these eight events have a better relationship with the shallow intraslab earthquakes, which have smaller SMGAs than that of inland crustal events with a similar seismic moment.

Asano et al. (2003) revealed that for those studied shallow intraslab earthquakes in Japan, the ratio SMGA/S_a decreases with focal depth, which suggests that the stress drop increases with focal depth. Figure 5b shows the relationship between the ratio SMGA/S_a and focal depth, and these eight Nantou events tend to follow a relationship

similar to inland crustal earthquakes (Miyake et al. 2003). However, Asano and Iwata (2011) derived the empirical relationship for inland crustal earthquakes in Japan and found that the stress drops on asperities increase by approximately 1 MPa for every 1 km depth. Thus, we further plot the stress drops on SMGA ($\Delta\sigma_{SMGA}$) against focal depths, as shown in Fig. 6. This plot shows that there is a clear depth dependency of the stress drop $\Delta\sigma_{SMGA}$ for these Nantou events, and we determined the relationship to be:

$$\Delta\sigma_{SMGA} = 0.47H + 15.20. \quad (5)$$

Here, H is the focal depth with a unit of km. This obtained empirical relationship is also plotted in Fig. 6 as the gray line, and its standard error is 4.13 MPa. Equation (5) indicates that in the Nantou area, the stress drops on SMGA of buried-fault events are essentially high (with an intercept value of 15.20) and increase with a slower rate of approximately 0.5 MPa for every 1 km depth. Asano and Iwata (2011) also found that the buried asperities seem to have larger stress drops than the surface-breaking asperities. This is consistent with the results of Kagawa et al. (2004), where the rupture area of the buried rupture earthquake was smaller and the deep asperity would have a larger stress drop and higher slip velocity. Furthermore, Radiguet et al. (2009) noted that both a blind fault and an immature fault would strengthen the strong ground shaking. Manighetti et al. (2007) concluded that the earthquake stress drop has a strong relationship with the structural maturity of the ruptured fault. Since these eight Nantou events all ruptured on the buried faults within a small region, it is reasonable to agree with
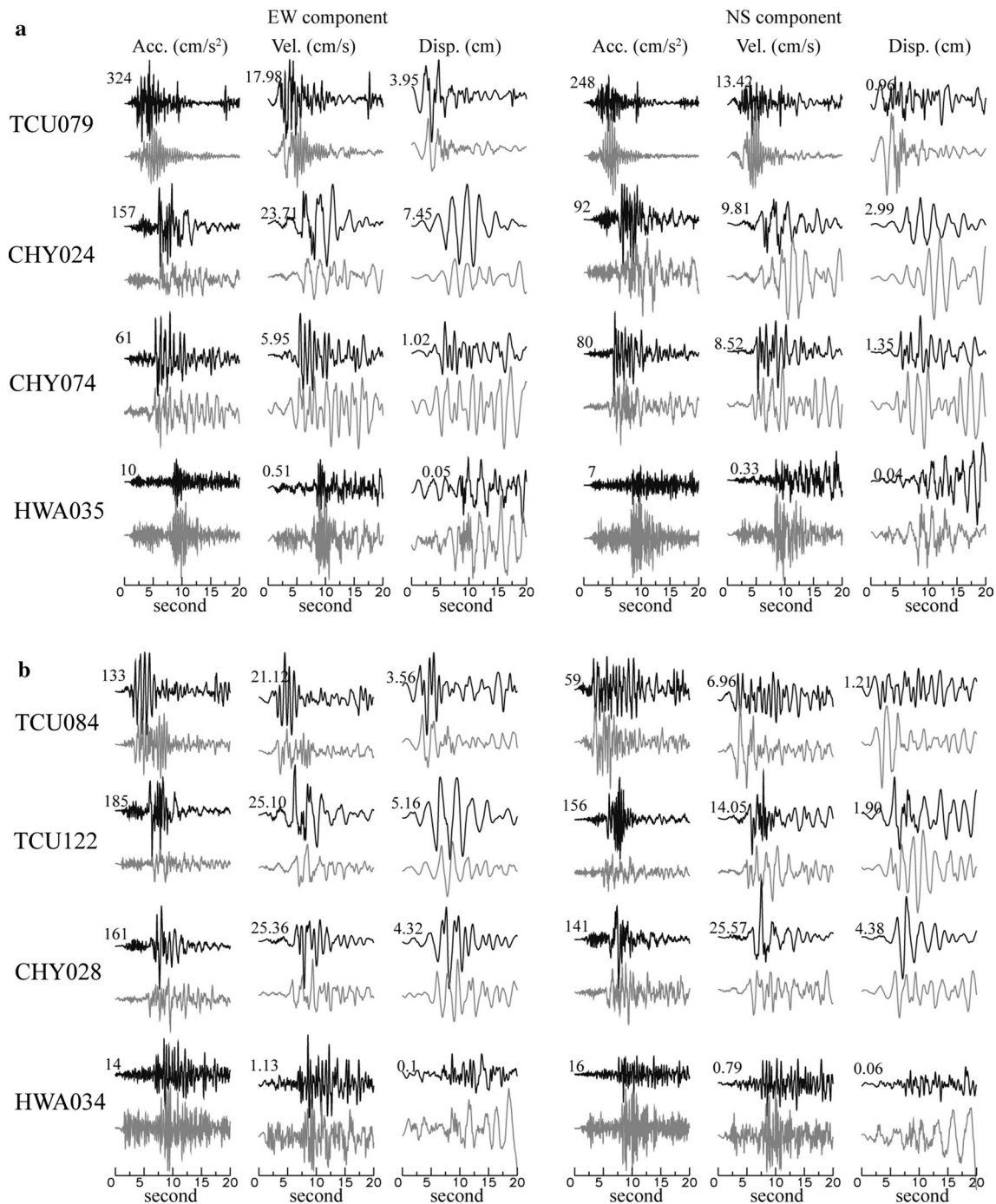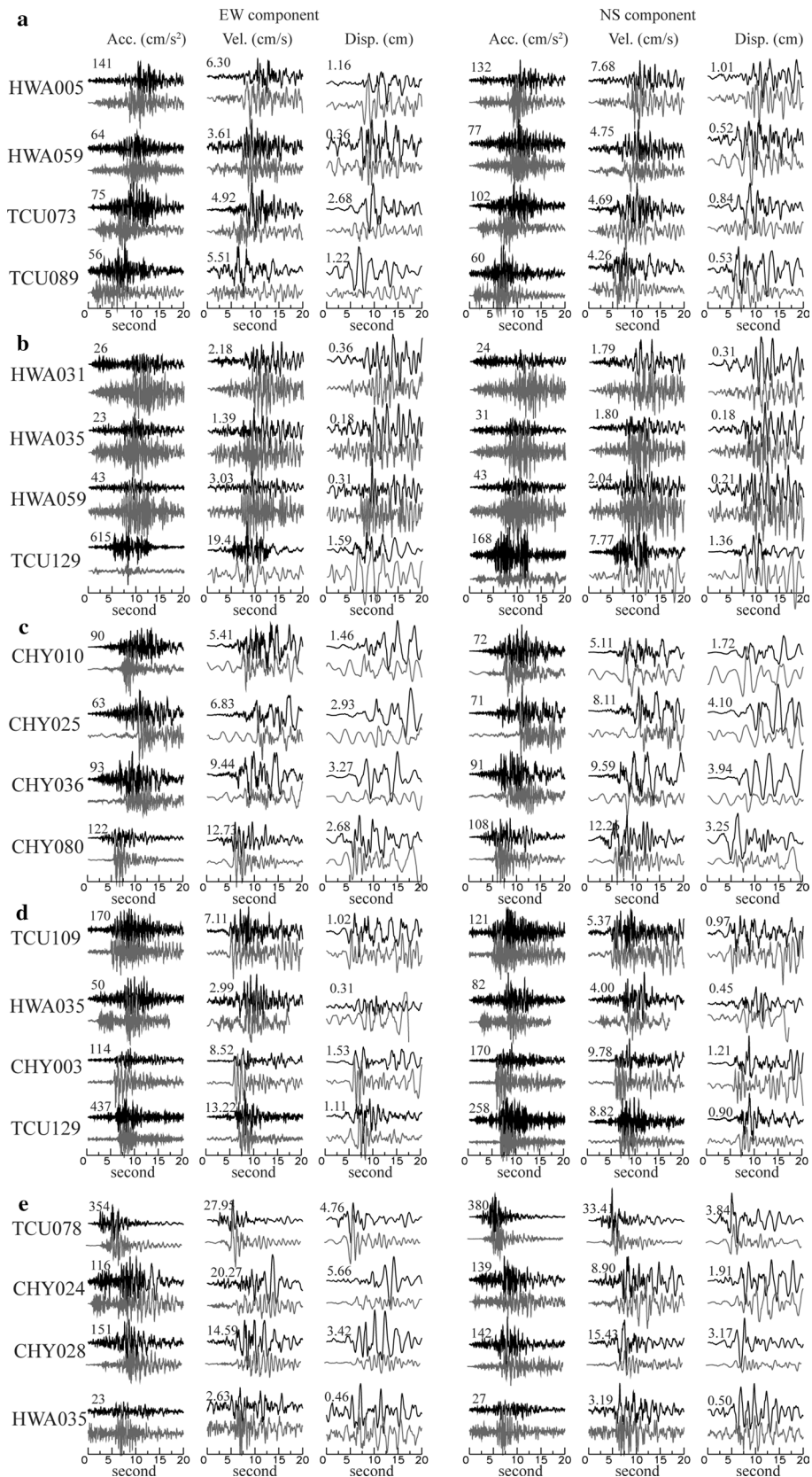
Wen *et al. Earth, Planets and Space* (2017) 69:132

Page 6 of 9

Fig. 3 Comparison of observed (black lines) and synthetic (gray lines) waveforms of event E1 at strong motion stations used for **a** the source modeling through the empirical Green's function method (solid triangles in Fig. 2a) and **b** forward ground motion simulations (open triangles in Fig. 2a), with the number indicating the maximum amplitudes of the observed records for acceleration (cm/s/s), velocity (cm/s) and displacement (cm)
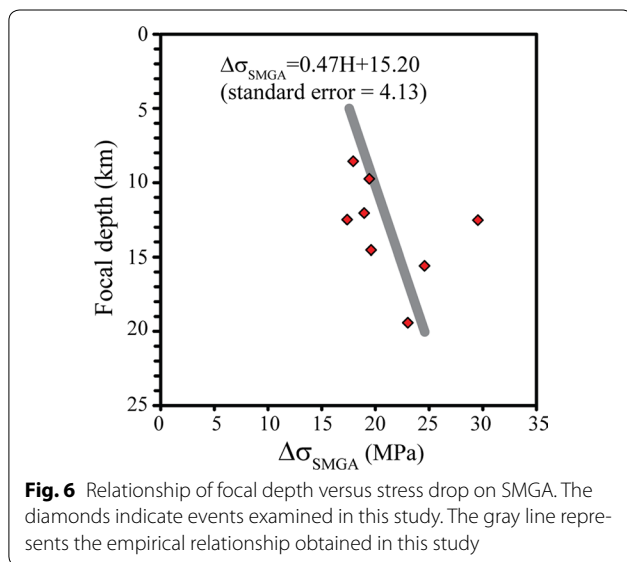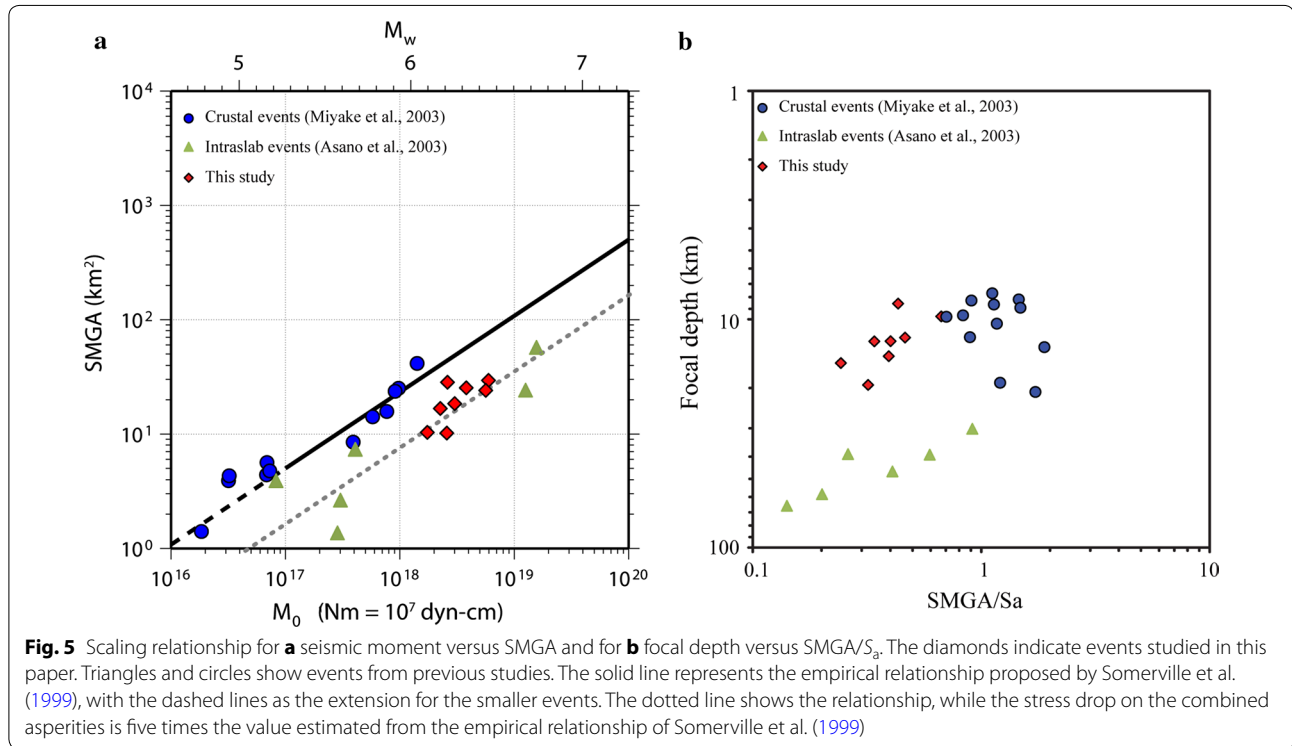
the suggestion of Wen et al. (2014) that the high stress drop of these eight Nantou events might be related to an immature buried fault. Since these adopted slip models were inverted from different data sets with various

techniques in a lower frequency range of 0.02–0.5 Hz, it might be better to derive the slip models with consistent analysis procedure for the further investigation and examination, such as relationship between the SMGA

Wen *et al. Earth, Planets and Space* (2017) 69:132

Page 7 of 9

Wen *et al. Earth, Planets and Space* (2017) 69:132

Page 8 of 9

(See figure on previous page.)

Fig. 4 Comparison of observed (black lines) and synthetic (gray lines) waveforms at the strong motion stations used for forward ground motion simulations (open triangles in Fig. 2) of **a** E2, **b** E3, **c** E4, **d** E5 and **e** E6 events, with the number indicating the maximum amplitudes of the observed records for acceleration (cm/s/s), velocity (cm/s) and displacement (cm)

Fig. 5 Scaling relationship for **a** seismic moment versus SMGA and for **b** focal depth versus SMGA/S_a. The diamonds indicate events studied in this paper. Triangles and circles show events from previous studies. The solid line represents the empirical relationship proposed by Somerville et al. (1999), with the dashed lines as the extension for the smaller events. The dotted line shows the relationship, while the stress drop on the combined asperities is five times the value estimated from the empirical relationship of Somerville et al. (1999)

Fig. 6 Relationship of focal depth versus stress drop on SMGA. The diamonds indicate events examined in this study. The gray line represents the empirical relationship obtained in this study

and characterized asperity, including the dimension and location. Although the number of the analyzed events was limited, the high stress drop and focal depth dependence are notable. Is this a special source characteristic of the Nantou area or a general property for Taiwan? More detailed and comprehensive investigations for other cases in Taiwan are needed to achieve a more confident conclusion.

In this study, we carried out the strong ground motion simulation and the integrated source analysis for the eight moderate-sized events that struck the Nantou area in 1999 and 2013. Lee et al. (2015) proposed that the moderate-to-large earthquakes in this region could be due to the accumulated stress at the eastern tip of the strong basement (named Peikang High; Tang 1977), where the stress convergent vector was nearly perpendicular to the eastern dipping ramp edge. The Nantou area is

Wen *et al. Earth, Planets and Space* (2017) 69:132

Page 9 of 9

a seismically active region, where several moderate-sized earthquakes have occurred and caused some disasters over the past century. Most of these events were attributed to the blind faults. Therefore, this unusual type of moderate-to-large event originating from buried faults should receive greater consideration in future earthquake scenario analyses for the mitigation of future seismic hazards.

Author details
[1] Department of Earth and Environmental Sciences, National Chung-Cheng University, Chia-Yi County 62102, Taiwan. [2] Sinotech Engineering Consultants, Inc., Taipei 11494, Taiwan.

Competing interests
The authors declare that they have no competing interests.

Consent for publication
Not applicable.

Ethics approval and consent to participate
Not applicable.

Publisher's Note
Springer Nature remains neutral with regard to jurisdictional claims in published maps and institutional affiliations.

References
Ammon JC, Ji C, Thio H, Robinson D, Ni S, Hjorleifsdottir V, Kanamori H, Lay T, Das S, Helmberger D, Ichinose G, Polet J, Wald D (2005) Rupture process of the 2004 Sumatra-Andaman earthquake. Science 308:1133–1139

Asano K, Iwata T (2011) Characterization of stress drops on asperities estimated from heterogeneous kinematic slip model for strong motion prediction for inland crustal earthquakes in Japan. Pure appl Geophys 168:105–116

Asano K, Iwata T, Irikura K (2003) Source characteristics of shallow intraslab earthquakes derived from strong-motion simulations. Earth Planets Space 55:e5–e8. doi:10.1186/BF03351744

Boatwright J (1988) The seismic radiation from composite models of faulting. Bull Seismol Soc Am 78:489–508

Brune JN (1970) Tectonic stress and the spectra of seismic shear waves from earthquakes. J Geophys Res 75:4997–5009

Brune JN (1971) Correction. J Geophys Res 76:5002

Cheng S-N, Yeh YT, Hsu M-T, Shin T-C (1999) Photo album of ten disastrous earthquakes in Taiwan. Central Weather Bureau and Institute of Earth Science, Academia Sinica, Taipei **(in Chinese)**

Chi WC, Dreger D (2004) Crustal deformation in Taiwan: results from finite source inversions of six Mw > 5:8 Chi-Chi aftershocks. J Geophys Res. doi: 10.1029/2003JB002606

Irikura K (1986) Prediction of strong acceleration motions using empirical Green's function. In: Proceedings of 7th Japan earthquake engineering symposium, pp 151–156, Tokyo, 10–12 Dec 1986

Irikura K, Kamae K (1994) Estimation of strong ground motion in broad-frequency band based on a seismic source scaling model and an empirical Green's function technique. Ann Geofis 37:1721–1743

Kagawa T, Irikura K, Somerville PG (2004) Differences in ground motion and fault rupture process between the surface and buried rupture earthquakes. Earth Planets Space 56(3):3–14. doi:10.1186/BF03352486

Kurahashi S, Irikura K (2010) Characterized source model for simulating strong ground motions during the 2008 Wenchuan earthquake. Bull Seismol Soc Am 100:2450–2475

Lay T, Wallace TC (1995) Modern global seismology. Academic Press, San Diego

Lee SJ, Yeh TY, Huang HH, Lin CH (2015) Numerical earthquake models of the 2013 Nantou, Taiwan, earthquake series: characteristics of source rupture processes, strong ground motions and their tectonic implication. J Asian Earth Sci 111:365–372. doi:10.1016/j.jseaes.2015.06.031

Madariaga R (1979) On the relation between seismic moment and stress drop in the presence of stress and strength heterogeneity. J Geophys Res 84:2243–2250

Manighetti I, Campillo M, Bouley S, Cotton F (2007) Earthquake scaling, fault segmentation, and structural maturity. Earth Planet Sci Lett 253:429–438

Miyake H, Iwata T, Irikura K (1999) Strong ground motion simulation and source modeling of the Kagoshima-ken Hokuseibu earthquakes of March 26 (M_{JMA} 6.5) and May 13 (M_{JMA} 6.3), 1997, using empirical Green's function method. Zisin 51:431–442 **(in Japanese with English abstract)**

Miyake H, Iwata T, Irikura K (2001) Estimation of rupture propagation direction and strong motion generation area from azimuth and distance dependence of source amplitude spectra. Geophys Res Lett 28:2727–2730

Miyake H, Iwata T, Irikura K (2003) Source characterization for broadband ground-motion simulation: kinematic heterogeneous source model and strong motion generation area. Bull Seismol Soc Am 93:2531–2545

Radiguet M, Cotton F, Manighetti I, Campillo M, Douglas J (2009) Dependency of near-field ground motions on the structural maturity of the ruptured faults. Bull Seismol Soc Am 99:2572–2581

Somerville P, Irikura K, Graves R, Sawada S, Wald D, Abrahamson N, Iwasaki Y, Kagawa T, Smith N, Kowada A (1999) Characterizing crustal earthquake slip models for the prediction of strong ground motion. Seismol Res Lett 70:59–80

Tang C-H (1977) Late miocene erosional unconformity on the subsurface Peikang High beneath the Chiayi-Yunlin, Coastal Plain, Taiwan. Mem Geol Soc China 2:155–167

Velasco AA, Ammon CJ, Lay T (1994) Empirical Green function deconvolution of broadband surface waves: rupture directivity of the 1992 Landers, California (Mw = 7.3) earthquake. Bull Seismol Soc Am 84:735–750

Wen Y-Y, Miyake H, Yen Y-T, Irikura K, Ching K-E (2014) Rupture directivity effect and stress heterogeneity of the 2013 Nantou blind-thrust earthquakes, Taiwan. Bull Seismol Soc Am 104:2933–2942. doi:10.1785/0120140109

Yen Y-T (2002) Slip distribution of Mw > 6:0 aftershocks of the 1999 Chi-Chi Taiwan earthquake. M.Sc. thesis, National Central University, Taiwan **(in Chinese)**

Yen Y-T, Asano K, Iwata I, Ma K-F, Wen Y-Y (2014) Source characteristics and strong-motion simulation of two moderate-size crustal earthquakes in Southwest Taiwan. In: Proceedings of 5th Asia conference on earthquake engineering, Taipei, ROC, paper no. 68